



HAL
open science

Beat-to-beat P-wave morphological variability in patients with paroxysmal atrial fibrillation: an in silico study

Simone Pezzuto, Ali Gharaviri, Ulrich Schotten, Mark Potse, Giulio Conte, Maria Luce Caputo, François Regoli, Rolf Krause, Angelo Auricchio

► To cite this version:

Simone Pezzuto, Ali Gharaviri, Ulrich Schotten, Mark Potse, Giulio Conte, et al.. Beat-to-beat P-wave morphological variability in patients with paroxysmal atrial fibrillation: an in silico study. EP-Europace, 2018, 20 (suppl 3), pp.iii26-iii35. 10.1093/europace/euy227. hal-01933828

HAL Id: hal-01933828

<https://inria.hal.science/hal-01933828v1>

Submitted on 28 Nov 2018

HAL is a multi-disciplinary open access archive for the deposit and dissemination of scientific research documents, whether they are published or not. The documents may come from teaching and research institutions in France or abroad, or from public or private research centers.

L'archive ouverte pluridisciplinaire **HAL**, est destinée au dépôt et à la diffusion de documents scientifiques de niveau recherche, publiés ou non, émanant des établissements d'enseignement et de recherche français ou étrangers, des laboratoires publics ou privés.

Beat-to-beat P-wave morphological variability in patients with paroxysmal AF: an in-silico study

Pezzuto S^{1,2,*}, Gharaviri A^{1,2}, Schotten U³, Potse M^{5,6,7}, Conte G^{1,7}, Caputo ML^{1,7}, Regoli F^{1,7}, Krause R^{1,2},
Auricchio A^{1,7}

¹Center for Computational Medicine in Cardiology,

²Institute of Computational Science, Università della Svizzera italiana, Lugano, Switzerland,

³Dept. of Physiology, Cardiovascular Research Institute Maastricht, Maastricht University, the Netherlands,

⁴CARMEN Research Team, INRIA, Talence, France,

⁵IHU Liryc, Electrophysiology and Heart Modeling Institute, Foundation Bordeaux Université Pessac, France,

⁶Univ. Bordeaux, IMB, UMR 5251, Talence, France,

⁷Fondazione Cardiocentro Ticino, Lugano, Switzerland.

*Corresponding author: Simone Pezzuto

E-mail: simone.pezzuto@usi.ch

Phone (office): +41 (0) 58 666 4976

Address of correspondance:

Institute of Computational Science,

Università della Svizzera italiana,

Via Giuseppe Buffi 13,

CH-6904 Lugano, Switzerland

Abstract and keywords

Aims. P-wave beat-to-beat morphological variability can identify patients prone to paroxysmal atrial fibrillation (AF). To date, no computational study has been carried out to mechanistically explain such finding. Aim of this study was to provide a pathophysiological explanation, by using a computer model of the human atria, of the correlation between P-wave beat-to-beat variability and the risk of AF.

Methods. A physiological variability in the earliest activation site (EAS), on a beat-to-beat basis, was introduced into a computer model of the human atria by randomizing the EAS location. A methodology for generating multi-scale, spatially-correlated regions of heterogeneous conduction was developed. P-wave variability in the presence of such regions was compared to a control case. Simulations were performed with an eikonal model, for the activation map, and with the lead field approach, for P-wave computation. The methodology was eventually compared to a reference monodomain simulation.

Results. A total of 60 P-waves were simulated for each sinus node exit location (12 in total), and for each of the 15 patterns of heterogeneous conduction automatically generated by the model. A P-wave beat-to-beat variability was observed in all cases. Variability was significantly increased in presence of heterogeneous slow conducting regions, up to 2-fold the variability in the control case. P-wave variability increased non-linearly with respect to the EAS variability and total area of slow conduction. Distribution of the heterogeneous conduction was more effective in increasing the variability when surrounded the EAS locations and the fast conducting bundles. P-waves simulated by the eikonal approach compared excellently to the monodomain-based ones.

Conclusions. P-wave variability in patients with paroxysmal AF could be explained by a variability in sinoatrial node exit location in combination with slow conducting regions.

Keywords. P-wave variability; P-wave morphology; Paroxysmal atrial fibrillation; inhomogeneous conduction; fibrosis; cosine distance

Condensed abstract

By using a generic computer model of the human atria, the P-wave variability on a beat-to-beat basis was explored. The variability increased in the presence of heterogeneous conduction, corroborating clinical observations.

What's new

- Simulation of beat-to-beat P-wave variability with physiological earliest activation site variability in the sinoatrial node region.
- Automatic generation of multi-scale, spatially-correlated heterogeneous conduction regions for realistic 3d atrial anatomy.
- In the presence of heterogeneous conduction in the atria, P-wave variability increases.
- P-wave and activation map compares excellently between the monodomain solution and the eikonal model with lead field approach.
- Robust methodology to measure the P-wave morphological variability.

Introduction

Pulmonary vein (PV) isolation is the treatment of choice in patients with paroxysmal and persistent atrial fibrillation¹. However, recurrence rate is still significant especially at mid- and long-term follow-up². Apart from reconnection of PV(s), alternative mechanism of atrial fibrillation recurrence may include persisting presence and extension of heterogeneous conduction areas (the substrate for reentry) and/or non-PV dependent triggered activity³. Areas of abnormal, heterogeneously distributed conduction within the atria have been well described in pre-clinical^{4,5} and clinical setting⁶, and can possibly represent the substrate for prolonged atrial conduction time (P-wave duration). Previous studies have indicated that both abnormal P-wave axis and long P-wave duration are strongly associated with an increased risk of AF⁷. More recently, dynamic morphological alteration of P wave (beat-to-beat P-wave morphology variability) has been reported by our group⁸ and others^{9,10}, and the combination of abnormal P wave duration and beat-to-beat variability has been shown to more effectively discriminate patients with history of AF from healthy age-matched subjects. This finding however has not been mechanistically well explained.

P-wave morphological variability, consistent with a beat-to-beat timeframe, could be related to a shift of the earliest activation site (EAS) in sinoatrial node (SAN) region¹¹. For instance, a shift in the EAS can be induced by exercise or drugs¹². SAN remodeling has been reported in patients with congestive heart failure¹³. Therefore, a possible mechanism explaining the difference in P-wave morphological variability between healthy subjects and patients with history of AF could be based on the interaction between EAS variability, physiologically always present, and the heterogeneity in conduction, generally increased in patient with history of AF.

By using a generic computer model of the human atria and torso, we aimed at reproducing the beat-to-beat variation of P-wave and the duration of P wave as clinically observed. We simulated P-waves as recorded on the 12-lead ECG, considering variation in the exit zone of the SAN, and modeling distribution and size of area of conduction heterogeneities generated by a novel automatic method in which spatial correlation, distribution, and size was prescribed.

Methods

Reference atrial model

We considered a reference anatomical model of the human atria previously built using MRI data from a normal subject¹⁴. The model contained several anatomical features such as the Bachmann's bundle, the crista terminalis, the interatrial bundles, and the pectinate muscles. All were designed by following anatomical studies¹⁵. Orientation bundles were manually added to define the fiber direction in the atrial tissue. A computational 3d structured grid with uniform spacing of 0.2mm was obtained from the anatomical model,

with roughly 5 million voxels in total. Each voxel was automatically marked with the corresponding anatomical region for the electrophysiological model parametrization (see Figure 1B).

Model of slow conducting regions

The slow conducting area in the model was defined by thresholding an automatically generated random field with given spatial correlation. More specifically, the random field was the average of two random Gaussian fields with different spatial correlation lengths, respectively set to 2cm and 4mm, thus to model organ-level and tissue-level inhomogeneity. The organ-level random field was sampled by using the truncated Karhunen-Loève expansion for a squared-exponential covariance function, with geodesic distance computed with the eikonal model¹⁶. The tissue-level random field was sampled by solving the linear fractional stochastic partial differential equation $\left(\frac{1}{\rho^2}I - \Delta\right)^{\alpha/2} u = W$, where W was white-noise, $\alpha = \nu + \frac{3}{2}$ with ν related to the spatial regularity of the field, and $\rho > 0$ related to the spatial correlation length. In practice, the partial differential equation smoothed the white-noise by introducing some spatial correlation of the order of ρ scale^{17,18}. The model was iteratively solved for increasing values of $\nu = \frac{4k-3}{2}$, $k = 1, 2, \dots$, and $\rho = \theta/2\sqrt{\nu}$. In the limit case, for $k \rightarrow \infty$, the random field has squared-exponential spatial correlation of parameter θ . The superposition of the random fields was eventually rescaled from 0 to 1. An illustrative example of such random field is provided in Figure 2A.

The area of slow conduction was finally defined as the region of the domain such that the random field was less than a threshold T . The threshold was selected by a bisection argument to ensure that the total volume of the slow conducting region was equal to a given fraction f of the total atrial volume (see Figure 2B). Bachmann's bundle, interatrial bundles and a portion of the RA (the intercaval region) were excluded from the threshold procedure but included in the random field generation.

Eikonal model for atrial activation

The electric activation of the atria was modeled by using the eikonal model¹⁹ with no curvature-correction:

$$\frac{\theta}{\sqrt{\beta}} \sqrt{\mathbf{G}_m \nabla \tau \cdot \nabla \tau} = 1,$$

where $\tau = \tau(x)$ was the activation time at some location x of the atria, θ was the conduction velocity scaling factor, β was the surface-to-volume ratio and \mathbf{G}_m was the monodomain electric conductivity tensor. The activation was initiated by setting τ to zero at a unique EAS. The electric conductivity tensor was transversely isotropic with major axis in the local fiber direction. The longitudinal and transverse intra- and extra-cellular electric conductivity were modeled with regional heterogeneity. The model contained 4 of such regions: an isotropic intercaval area in the right atrium (0.75 mS/cm monodomain conductivity for both longitudinal and transversal); the Bachmann's bundle and atrial connections (4.5 mS/cm and 0.72 mS/cm respectively longitudinally and transversely); tissue with oriented bundles (1.5 mS/cm and 0.72 mS/cm); and a slow

conducting area (1 mS/cm and 0.28 mS/cm). The surface-to-volume ratio was set to 800 cm⁻¹ everywhere except in the slow conducting region, where it was doubled. The conduction velocity scaling factor (units cm · ms⁻¹ · mS^{-1/2}) and the transmembrane potential template were pre-computed with a single fiber monodomain simulation using the Courtemanche ionic model²⁰. A summary of the parameters adopted in the simulation is found in Table 1.

P-wave simulation

The 12-lead surface ECG was simulated by using the formula

$$V(t) = \int_{\Omega} \mathbf{G}_i \nabla V_m \cdot \nabla Z \, dx,$$

where Ω was the atrial tissue, $V_m(x, t)$ was the transmembrane potential, \mathbf{G}_i was the intracellular electric conductivity, and $Z(x)$ was a precomputed lead field. For each lead, the bidomain problem in the full torso was solved for the lead field $Z = Z(x)$ by injecting a unit current at the electrode locations. The torso, heterogeneous and anisotropic, included atrial and ventricular tissue, blood cavities, lungs, skeletal muscles. The transmembrane potential was set to $V_m(x, t) = U(t - \tau(x))$, with U a pre-computed action potential template. An efficient implementation of the ECG computation in combination with the eikonal solution, on GPGPU architecture, was provided by the software Propeiko²¹.

Randomized early activation site location

The electric activation was triggered at a single EAS location for each beat, located in the sinoatrial node (SAN) area, on the right atrium (RA). From an anatomical viewpoint, the SAN is functionally isolated for the atrial myocardium, except for several sinoatrial connection pathways (SACP) uniformly distributed around the SAN. A total of 12 SAN locations were considered in the atrial model, as depicted in Figure 1A. These were manually placed on the RA starting from the superior vena cava (SVC) and moving towards the inferior vena cava (IVC). The selected locations were consistent with histological studies²² and previous in-silico investigations¹¹.

To enable a beat-to-beat variability of the activation, the EAS location was modeled as a uniform random variable of spherical shape and intersected with the right-atrial tissue. The sphere was centered at a specific SAN locations with a predefined radius. The sampling radius was set from 1mm up to 5mm.

P-wave analysis

For each sampled EAS location, the corresponding P-wave was computed. The P-wave morphological variability was evaluated with two approaches: one based on the spectral radius of the cosine distance matrix, and the second based on the standard deviation of the P-waves. Denoting by $V_i(t)$ the i -th P-wave, $i = 1, \dots, N$, the cosine distance between the i -th and j -th P-wave was as follows

$$d_{\cos}(V_i, V_j) = \frac{1}{\pi} \cos^{-1} \left(\frac{\int_0^T V_i(t) V_j(t) dt}{\left(\int_0^T V_i^2(t) dt \right)^{1/2} \left(\int_0^T V_j^2(t) dt \right)^{1/2}} \right).$$

Then, the variability v_{\cos} was evaluated as the largest absolute value of the eigenvalues of the matrix $D_{ij} = d_{\cos}(V_i, V_j)$, i.e. its spectral radius: $\max_{i=1, \dots, N} |\lambda_i(D)|$, divided by the number of eigenvalues or, equivalently, the number of beats.

With the second methodology, the variability was assessed from the p -norm (with $p = 1$ or $p = \infty$) of the standard deviation of the P-wave sample

$$v_p = \frac{\left\| \sqrt{\frac{1}{N-1} \sum_{i=1}^N (V_i(t) - \bar{V}(t))^2} \right\|_{L^p(O,T)}}{\|\bar{V}\|_{L^p(O,T)}},$$

where $\bar{V}(t) = \frac{1}{N} \sum_{i=1}^N V_i(t)$ was the average P-wave. Both measures of variability were non-dimensional.

Monodomain simulations

An activation map and corresponding surface ECG was computed with the monodomain model and compared to the eikonal model. The monodomain solver was Propag²³, using the same computational grid and the same parameters, when applicable. The comparison was performed in the control case and with heterogeneous conduction, pacing from a fixed EAS location (SAN01). In the monodomain model, a current of $150 \mu\text{A}/\text{cm}^3$ was applied for 2ms in a 1mm^3 volume centered at the EAS location. In the eikonal model, we simply set the activation time to the onset value at the EAS location. The P-wave was computed with the lead field approach for the eikonal solution, and with the bidomain model in the torso for the monodomain solution. The torso geometry for the bidomain model was as for the lead field computation. Sampling time was 0.2ms in both cases (time-step for explicit time integration in the monodomain model was 0.01ms).

Results

Comparison between the eikonal and the monodomain model

An activation map and the corresponding P-wave was computed by using either the eikonal or the monodomain model, both in control case and with slow conducting areas (30% area, pattern 3). In the eikonal model, the parameter θ was globally adjusted to reflect the average conduction velocity observed in the monodomain case ($\theta = 1.519$ in control case and $\theta = 1.4273$ for heterogeneous conduction). A fixed delay in activation of 2ms was introduced in the eikonal model to accommodate the delay in activation in the monodomain case, due to the current injection. Results are presented in Figure 3.

In control case, the correlation of between the activation maps of the two models was 0.999, the RMSE was 1.2ms and the 99th percentile of the absolute error was 2.9ms. In patchy conduction case, the correlation,

the RMSE and the 99th percentile of the error were respectively 0.998, 2.3ms and 6.4ms. By using the reference parameter $\theta = 1.6176$, obtained with a high resolution 1d monodomain simulation, the root-mean-square error (RMSE) in control case was increased to 5.1ms. In all cases, the monodomain activation resulted slightly longer than the eikonal one.

The cosine distance between the P-waves in control case was between 0.02 (lead V6) and 0.08 (lead V3). In lead II (maximum amplitude lead), the cosine distance was 0.02. For the heterogeneous conduction case, the cosine distance was 0.016 in lead II, and ranged from 0.015 (aVL) to 0.093 (V3). In terms of amplitude and duration, P-waves were indistinguishable. The RMSE was $5.4 \cdot 10^{-3}$ mV on average in both cases. The monodomain solution took 100s on CSCS Piz Daint cluster using 4 nodes. The eikonal solution took 20sec in total on a single GPGPU (Nvidia GTX1080).

P-waves simulation

A total of 60 beats for each of the 12 SAN exit locations were simulated for the control case (no slow conduction region) and for 15 different heterogeneous conduction patterns. For each random pattern case (see Figure 2C-E, on the right), the fraction of slow conducting tissue was set from 20% up to 60%, with increments of 10% (Figure 2B). In total, 16 configurations were simulated (including the control case) for a total of 11'520 P-waves. The EAS locations, sampled around each SAN, were different from case to case. Simulations were performed with the same setup as above (20sec each on a local workstation).

Variability in control and with heterogeneous conduction

In control case, the average P-wave amplitude and duration in lead II were 0.21 ± 0.07 mV and 140.2 ± 5.2 ms, respectively. The P-wave variability using the cosine distance was 0.075 ± 0.043 . Variability was comparable among SAN exit locations, except for EASs around SAN11 and SAN12, for which the variability was 2-fold larger. On average, lead V3 reported the largest variability (0.124 ± 0.036), while V6 the smallest one (0.039 ± 0.013). The v_1 and the v_∞ distance were respectively 0.20 ± 0.137 and 0.25 ± 0.138 . A similar trend to cosine distance was observed.

In Figure 4 we report a comparison between the control and case 3 with 40% area of heterogeneous conduction. A similar analysis was performed for all the other cases. Overall, the variability was larger in the presence of slow conducting regions, of a factor of 2 on average. In Figure 4A, we report the distribution of the entries of the cosine distance matrix, that is the cosine distance between all possible pairs of simulated P-waves. The histogram showed a significantly increased spread of cosine distance in the heterogeneous case, in all the leads. The distribution of distances was bell-shaped (as in control) but shifted to the right and with significantly fatter tails. The increase in variability was also confirmed by the box-plot analysis (Figure 4B).

In Figure 4C and D we superimpose the P-waves to highlight the variability. The average P-wave in the control case was very close (in amplitude and morphology) to the P-wave produced by pacing exactly at the SAN exit location. In the presence of slow conducting regions, the average P-wave was smoother and with lower amplitude than the P-wave obtained as above.

Finally, in Figure 5A, we report the cosine distance between all P-wave pairs, as a function of the (Euclidean) distance between the corresponding EASs. In the heterogeneous case, the variability versus EAS distance relationship was steeper and less sharp than the control case.

Effect of distribution and area of inhomogeneous conduction

The effect of slow conduction distribution on the P-wave variability was explored by increasing the fraction of slow conducting region for 3 different patterns. Results are reported in Figure 5B and Figure 6. In general, an increasing area of slow conduction led to an increase of variability. For some pattern (e.g. pattern 1 and pacing around SAN02, or pattern 2 with pacing around SAN03), the variability v_{\cos} was maximum for a fraction of 20% and reducing for larger values. The cosine variability was also significantly affected by the distribution of the slow conducting region: pacing around SAN03, variability in lead II was 2-fold the control case in case 3 with 40% area, while it was 1.5-fold in case 2 and comparable to control in case 1. Only very few cases reported a reduced variability with respect to control case. This occurred when activation around SAN12, especially for case 3.

Effect of filtering on variability

The analysis was repeated with filtering applied to all the P-wave samples prior the evaluation of the variability. The filter was a 5th order Butterworth filter with cut-off frequency of 40Hz. With filtering, the cosine variability was 33% lower in control case, and from 16% to 46% lower in the inhomogeneous cases. In general, the cosine variability with filter applied was still larger than the control case, corroborating the above analysis. More specifically, the ratio in variability (heterogeneous over control) was higher with filter applied (from 1.3x to 2.8x versus 1.1x to 2.6x in absence of filtering).

Discussion

This manuscript presents several novelties. First, we developed a novel approach to generate areas of conduction heterogeneities in the atria with a given spatial correlation, distribution, and size. Secondly, we could simulate a beat-to-beat P-wave variability as reported by clinical observation in healthy subjects and in patients with paroxysmal AF⁸, by adopting a physiologically-motivated variation of SAN exit location which has not been previously accounted for in the literature, to the best of our knowledge. Finally, we compared the eikonal model with the lead field approach for P-wave computation against the monodomain model.

Our model suggested that the beat-to-beat variability is related to presence and quantity of heterogeneous conduction, in combination with the intrinsic variability in the EAS location in the SAN region²⁴. The numerical investigation showed, as expected, that the variability increases with respect to the EAS variability, in both control case and with heterogeneous conduction. In the latter case, however, the variability grows more rapidly than the former, as certified by the results in Figure 5. We also observed that for the sampling radius of the EASs had a modest effect on variability for values larger than 4 mm.

The EAS physiological variability alone can only partially account for the difference in P-wave morphological variability between healthy subjects and patients with history of AF. We found that the P-wave variability is also a complex function of distribution and area of slow conducting region. Moreover, its magnitude also depends from which lead is measured, and whether a filtering procedure was performed prior the analysis. In addition, there is no clear definition of variability, mathematically speaking. Despite these difficulties, we have found a consistent increase of variability in the presence of slow conducting regions, compared to the control case, except in a very few cases. For instance, the variability in the presence of slow conducting regions was comparable or slightly lower than the control case when activation occurred around SAN11 and SAN12, which are close to IVC. Interestingly, the variability in control was already very large, probably because these locations are close to the interatrial bundles (IAB). Moreover, none of the analyzed patterns had an extensive slow conducting area in the region of these SAN exit locations.

The presence of slow conducting region around the SAN exit location only partially explains the increase in P-wave variability. In the experiments, another important factor was the presence of such region close to the IABs and the Bachmann's bundle (BB), and its distribution on the left atrium. In such cases, the P-wave variability could be explained by a shift of some portions of the P-wave, and an increased fragmentation. In fact, the slow conducting region was present in all the patterns around SAN01 to SAN03 and the BB.

Another interesting observation is that the P-wave variability increased with the fraction of slow conducting region but, in some cases, for very large values of fraction the variability declined (see Figure 5B, case 2). It is reasonable to argue that under such circumstances the variability is comparable to the control case, because heterogeneity at organ-scale is reduced, albeit heterogeneity at tissue-scale may still be large. This may also indicate that intermediate fractions of slow conducting region (or severe heterogeneity at organ-scale) might characterize the electric substrate of patients with paroxysmal AF. In this respect, the P-wave morphological variability in sinus rhythm may provide additional insight on the stage of AF, from paroxysmal to persistent²⁵.

Importance of heterogenous conduction

Heterogeneous conduction in the atria has been already reported and explored by other authors in the literature, especially as a possible mechanism to sustain and enhance AF³. These regions have been identified as fibrotic, and they are generally obtained from imaging techniques⁵, in patient-specific context. Our novel

methodology significantly expands the previous knowledge as we proposed a general methodology to automatically generate such fibrotic regions, by requiring a specific spatial correlation and total fibrotic area. The generated patterns closely resemble those available in the literature^{5,6}. The key aspect of our approach was the enforcement of a spatial correlation at multiple scales. It is reasonable to argue that the formation of fibrosis is spatially-correlated at the tissue-level, due to cellular coupling. An organ-scale spatial correlation may instead be favored by mechanical coupling, for instance. Unfortunately, to the best of our knowledge, spatial correlation of such fibrotic regions has never been quantitatively investigated in the literature.

Variability measure

Conte et al.⁸ suggested the use of the Euclidean distance between one beat and the successive one, normalized with respect to the current beat. An overall assessment of the variability was eventually based on statistics of the Euclidean distance time series. While such measure may be practical in a clinical context, it comes with some limitations: it is not a distance in strictly mathematical terms (it misses symmetry), and it is not independent on the order of the beats. In this work, we proposed two different methods to compute the P-wave variability which they both overcame the mentioned limitations. Interestingly, we found that the v_{\cos} variability measure is often very close (relative difference less than 5%) to the mean value of the entries of the distance matrix, which is straightforward to compute. This is a consequence of the positivity of the matrix (all entries are non-negative), and the Frobenius-Perron Theorem: the dominant eigenvalue, which is non-negative and corresponds to the spectral radius, is bounded by the minimum (from below) and the maximum (from above) of the sum by row of the matrix entries; dividing by the sample size, we bound v_{\cos} with minimum and maximum average (by row).

We observed minor differences in the choice of the distance, albeit they have different properties. The cosine distance is suitable to measure morphological (or shape) differences between two P-waves; it is invariant under scaling, i.e. $d_{\cos}(aV_i, bV_j) = d_{\cos}(V_i, V_j)$ for any a, b . However, the cosine distance is not invariant under shift in amplitude and time. This may represent an issue in clinical setting.

The v_p -variability measure may highlight localized differences in P-wave morphology. An example is provided by Figure 4. The shaded area is region spanned by ± 2 standard deviations around the average P-wave. An interesting interpretation of the v_p -variability measure is the following: for $p = 1$, the variability is half of the shaded area; for $p = \infty$, the variability is the maximum deviation in absolute value from the average P-wave. Clearly, the v_p -variability is unaffected by a constant change of the baseline, but it still may be affected by shifts in the time domain.

Suitability of the eikonal model

We assessed the P-wave variability analysis by using the eikonal model for the activation map and the lead field approach for the P-wave simulation. The main advantage of the eikonal approach is its computational

efficiency: for the atrial model adopted in this work, a full P-wave simulation took less than half a minute on a single GPGPU. Incidentally, the total cost could have been reduced to 5sec by using a coarser computational grid, but in this case the comparison to the reference monodomain solution would have been less favorable (not shown). In a previous study from our group we compared the eikonal-based method against the full monodomain model, in terms of activation map and ECG, for the ventricular activation, obtaining very good agreement²¹. In this work we extended the analysis to the atrial activation and the P-wave in sinus rhythm (SR), confirming the appropriateness of the methodology for both the control case and with patchy slow conduction. The suitability of the eikonal model was also explored previously by other group with convincing results^{26,27}, albeit they focused only on the activation map.

The parameter θ in the eikonal simulations required an adjustment for matching the corresponding monodomain simulation. The reason is the relatively large numerical error in the monodomain case. Using a standard finite difference discretization at 0.2mm voxel size, the conduction velocity is generally 10% to 20% slower (depending on the wave-front thickness) than the converged value²⁸. This is consistent with θ values we found. In this respect, we believe that the eikonal model was more accurate (in terms of conduction velocity) than the monodomain model for the presented simulations. However, if the slow conduction region were modeled by removing computational cells from the active tissue, or by substituting a fraction of cells with fibroblasts²⁹, the classic eikonal approach would have not been suitable.

The rapidity of eikonal model for atrial simulations potentially enables multi-fidelity parameter identification and uncertainty quantification in SR^{16,30}. The personalization process of the atrial model is of paramount importance for clinical application, and this can be performed in SR.

Nonetheless, the eikonal model comes with significant approximations with respect to the monodomain or bidomain model. In its original form, it is not suitable for atrial fibrillation (AF) simulations, lacking re-excitability of the tissue, thus limiting its clinical applicability. However, modifications of the original model have been proposed to include action potential refractoriness²⁶ and, more recently, conduction velocity dependency on the cycle length³¹. Finally, the lead field approach is fully equivalent to simulating the P-wave using the bidomain model in the torso with a precomputed transmembrane potential. It includes both heterogeneity and anisotropy of the torso and heart, and it is a computationally efficient method when the extracellular potential is required only at a few given locations, such as the standard 12-lead ECG.

Limitations

This study certainly comes with some limitations. The effect of the distribution of heterogenous conduction was analyzed for only 3 patterns. No distinction was made between LA and RA in the generation of the random field, although a difference in area and distribution between the two chambers might be present. In the model, we assumed a sharp reduction in the intracellular conductivity within the slow conducting regions,

thus to produce a reduced conduction velocity. The assumption was loosely based on experimental data. Some groups³ have proposed a similar approach to model fibrotic regions, but there is no consensus on how to select the parameters.

Conclusions

In this work, we showed that the morphological P-wave variability could be explained by an intrinsic variability in the SAN exit points in combination with a diffuse and heterogenous conduction in the atrial tissue. The larger the slow conducting area is, the larger the variability. The heterogenous conduction may be associated to fibrotic regions.

By using the same anatomy and slow conduction area in the monodomain AF simulations, we observed an increase in the variability of AF conduction pattern. An increase in the slow conducting area led to an increase in AF conduction pattern complexity. Hence, this might be an important step forward to help the outcome of AF computer models become closer to clinical and experimental recordings.

Paroxysmal AF has been traditionally assumed to originate from a combination of triggered activity and reentry circuits mediated by the atrial refractory period and the conduction velocity. Computer modeling is a recognized tool of utmost importance to provide new mechanistic insights of arrhythmias behavior and to identify the coexistence of different mechanisms responsible for the arrhythmia development. Indeed, for paroxysmal AF, the combination of fibrosis and variability in the SAN exit points might provide information on the arrhythmia stage, which is important while assessing pulmonary vein isolation outcomes. Moreover, P-wave beat-to-beat variability can be used to identify patients with asymptomatic episodes of paroxysmal AF and can drive the subsequent diagnostic and therapeutic management.

Further computational studies and patient-specific approaches are needed to address prediction of optimal pharmacological drug agents and ablation sites able to decrease P-wave beat-to-beat morphological variability and avoid episodes of paroxysmal AF.

Acknowledgments

The authors acknowledge financial support by the Theo Rossi di Montelera Foundation, the Metis Foundation Sergio Mantegazza, the Fidinam Foundation, and the Horten Foundation to the Center for Computational Medicine in Cardiology. This work was also supported by grants from the Swiss National Supercomputing Centre (CSCS) under project ID s778.

References

1. Haïssaguerre M, Jaïs P, Shah DC, Takahashi A, Hocini M, Quiniou G, *et al.* Spontaneous Initiation of

- Atrial Fibrillation by Ectopic Beats Originating in the Pulmonary Veins. *N Engl J Med* 1998;**339**:659–66.
2. Verma A, Jiang C, Betts TR, Chen J, Deisenhofer I, Mantovan R, *et al.* Approaches to Catheter Ablation for Persistent Atrial Fibrillation. *N Engl J Med* 2015;**372**:1812–22.
 3. Zahid S, Cochet H, Boyle PM, Schwarz EL, Whyte KN, Vigmond EJ, *et al.* Patient-derived models link re-entrant driver localization in atrial fibrillation to fibrosis spatial pattern. *Cardiovasc Res* 2016;**110**:443–54.
 4. Akoum N, Daccarett M, McGann C, Segerson N, Vergara G, Kuppahally S, *et al.* Atrial fibrosis helps select the appropriate patient and strategy in catheter ablation of atrial fibrillation: A DE-MRI guided approach. *J Cardiovasc Electrophysiol* 2011;**22**:16–22.
 5. Marrouche NF, Wilber D, Hindricks G, Jais P, Akoum N, Marchlinski F, *et al.* Association of Atrial Tissue Fibrosis Identified by Delayed Enhancement MRI and Atrial Fibrillation Catheter Ablation. *JAMA* 2014;**311**:498.
 6. Fukumoto K, Habibi M, Ipek EG, Zahid S, Khurram IM, Zimmerman SL, *et al.* Association of Left Atrial Local Conduction Velocity With Late Gadolinium Enhancement on Cardiac Magnetic Resonance in Patients With Atrial Fibrillation. *Circ Arrhythmia Electrophysiol* 2016;**9**:e002897.
 7. German DM, Kabir MM, Dewland TA, Henrikson CA, Tereshchenko LG. Atrial Fibrillation Predictors: Importance of the Electrocardiogram. *Ann Noninvasive Electrocardiol* 2016;**21**:20–9.
 8. Conte G, Luca A, Yazdani S, Caputo ML, Regoli F, Moccetti T, *et al.* Usefulness of P-Wave Duration and Morphologic Variability to Identify Patients Prone to Paroxysmal Atrial Fibrillation. *Am J Cardiol* 2017;**119**:275–9.
 9. Filos D, Chouvarda I, Tachmatzidis D, Vassilikos V, Maglaveras N. Beat-to-beat P-wave morphology as a predictor of paroxysmal atrial fibrillation. *Comput Methods Programs Biomed Elsevier Ireland Ltd*; 2017;**151**:111–21.
 10. Huo Y, Holmqvist F, Carlson J, Gaspar T, Hindricks G, Piorkowski C, *et al.* Variability of P-wave morphology predicts the outcome of circumferential pulmonary vein isolation in patients with recurrent atrial fibrillation. *J Electrocardiol Elsevier Inc.*; 2015;**48**:218–25.
 11. Loewe A, Krueger MW, Holmqvist F, Dössel O, Seemann G, Platonov PG. Influence of the earliest right atrial activation site and its proximity to interatrial connections on P-wave morphology. *Europace* 2016;**18**:35–43.
 12. Löbe S, Kosiuk J, John S, Hilbert S, Hindricks G, Bollmann A. Sinus node modification with an ultra high-density electroanatomical mapping system in inappropriate sinus tachycardia. *EP Eur* 2017;**19**:1656–1656.
 13. Sanders P. Remodeling of Sinus Node Function in Patients With Congestive Heart Failure: Reduction in Sinus Node Reserve. *Circulation* 2004;**110**:897–903.
 14. Potse M, Lankveld TAR, Zeemering S, Dagnelie PC, Stehouwer CDA, Henry RM, *et al.* P-wave complexity in normal subjects and computer models. *J Electrocardiol* 2016;**49**:545–53.
 15. Ho SY, Anderson RH, Sanchez-Quintana D. Atrial structure and fibres: morphologic bases of atrial conduction. *Cardiovasc Res* 2002;**54**:325–36.
 16. Quaglino A, Pezzuto S, Koutsourelakis P-S, Auricchio A, Krause R. Fast uncertainty quantification of activation sequences in patient-specific cardiac electrophysiology meeting clinical time constraints. *Int j numer method biomed eng* 2018;1–28.
 17. Lindgren F, Rue H, Lindström J. An explicit link between Gaussian fields and Gaussian Markov

random fields: the stochastic partial differential equation approach. *J R Stat Soc Ser B (Statistical Methodol)* 2011;**73**:423–98.

18. Stein ML. Interpolation of spatial data: some theory for kriging. New York: Springer Science & Business Media; 2012.
19. Colli Franzone P, Guerri L, Pennacchio M, Taccardi B. Spread of excitation in 3-D models of the anisotropic cardiac tissue. II. Effects of fiber architecture and ventricular geometry. *Math. Biosci.* 1998. p. 131–71.
20. Courtemanche M, Ramirez RJ, Nattel S. Ionic mechanisms underlying human atrial action potential properties: insights from a mathematical model. *Am J Physiol Circ Physiol* 1998;**275**:H301–21.
21. Pezzuto S, Kal’avský P, Potse M, Prinzen FW, Auricchio A, Krause R. Evaluation of a Rapid Anisotropic Model for ECG Simulation. *Front Physiol* 2017;**8**.
22. Csepe TA, Zhao J, Sul L V., Wang Y, Hansen BJ, Li N, *et al.* Novel application of 3D contrast-enhanced CMR to define fibrotic structure of the human sinoatrial node in vivo. *Eur Hear J – Cardiovasc Imaging* 2017;**18**:jew304.
23. Krause D, Potse M, Dickopf T, Krause R, Auricchio A, Prinzen F. Hybrid Parallelization of a Large-Scale Heart Model. 2012. p. 120–32.
24. Li N, Hansen BJ, Csepe TA, Zhao J, Ignozzi AJ, Sul L V., *et al.* Redundant and diverse intranodal pacemakers and conduction pathways protect the human sinoatrial node from failure. *Sci Transl Med* 2017;**9**:eaam5607.
25. Schotten U, Verheule S, Kirchhof P, Goette A. Pathophysiological Mechanisms of Atrial Fibrillation: A Translational Appraisal. *Physiol Rev* 2011;**91**:265–325.
26. Jacquemet V. An Eikonal Approach for the Initiation of Reentrant Cardiac Propagation in Reaction–Diffusion Models. *IEEE Trans Biomed Eng* 2010;**57**:2090–8.
27. Krueger MW, Schulze WHW, Rhode KS, Razavi R, Seemann G, Dössel O. Towards personalized clinical in-silico modeling of atrial anatomy and electrophysiology. *Med Biol Eng Comput* 2013;**51**:1251–60.
28. Pezzuto S, Hake J, Sundnes JS. Space-discretization error analysis and stabilization schemes for conduction velocity in cardiac electrophysiology. *Int j numer method biomed eng* 2016;**32**:e02762.
29. Sridhar S, Vandersickel N, Panfilov A V. Effect of myocyte-fibroblast coupling on the onset of pathological dynamics in a model of ventricular tissue. *Sci Rep* Nature Publishing Group; 2017;**7**:40985.
30. Konukoglu E, Relan J, Cilingir U, Menze BH, Chinchapatnam P, Jadidi A, *et al.* Efficient probabilistic model personalization integrating uncertainty on data and parameters: Application to Eikonal-Diffusion models in cardiac electrophysiology. *Prog Biophys Mol Biol* 2011;**107**:134–46.
31. Corrado C, Zemzemi N. A conduction velocity adapted eikonal model for electrophysiology problems with re-excitability evaluation. *Med Image Anal* 2018;**43**:186–97.

Figures

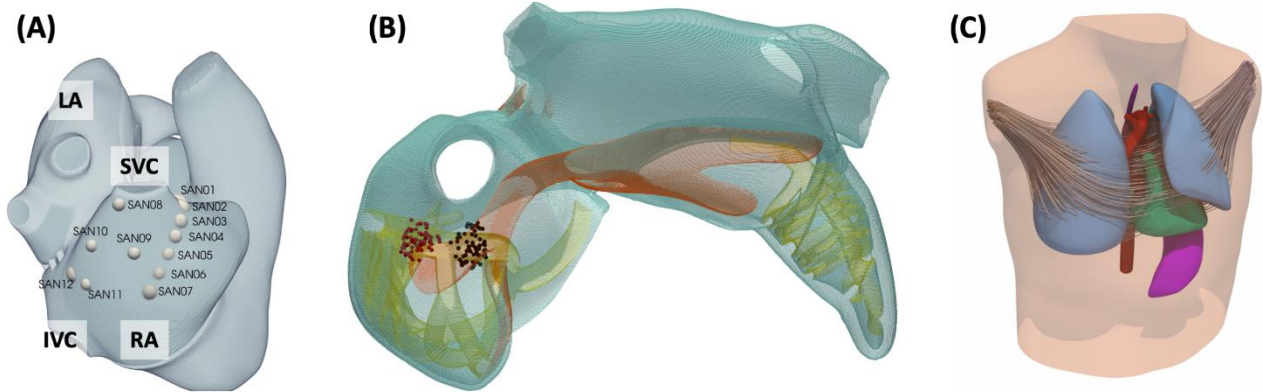
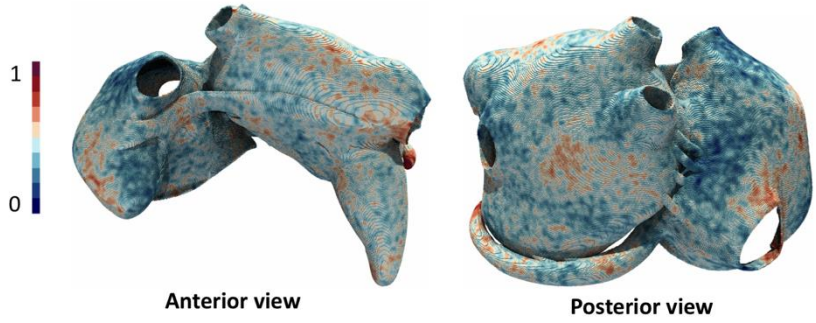
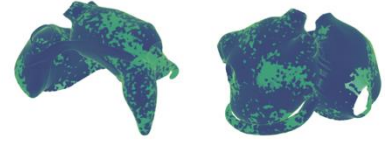


Figure 1 (A) Location of the SAN exit location on the left atrium. (B) Anatomical model of the atria in use for the simulations, with oriented bundles (in yellow), Bachmann's bundle and interatrial bundles (in orange), and an example of EASs locations around SAN01 and SAN03 (60 samples each in total). (C) Lead field for lead II, with torso anatomy.

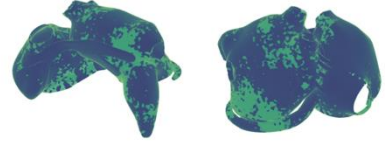
(A) Background random field (pattern 1)



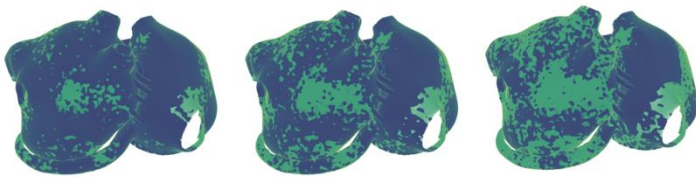
(C) Pattern 1, 30% SCR



(D) Pattern 2, 30% SCR



(B) Pattern 1, from 20%, 40% and 60% SCR



(E) Pattern 3, 30% SCR

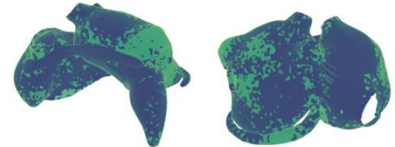


Figure 2 Generation of slow conduction regions (SCRs) for various patterns and densities.. On the top left, the background random field for pattern 1 is represented, with low values towards blue and high values towards the red. On bottom left, the result of the thresholding procedure to extract the SCR at different level of total area (20%, 40% and 60%).. On the right, all the patterns considered in this study, represented only for 30% of SCR. . SCR is in bright green in all figures.

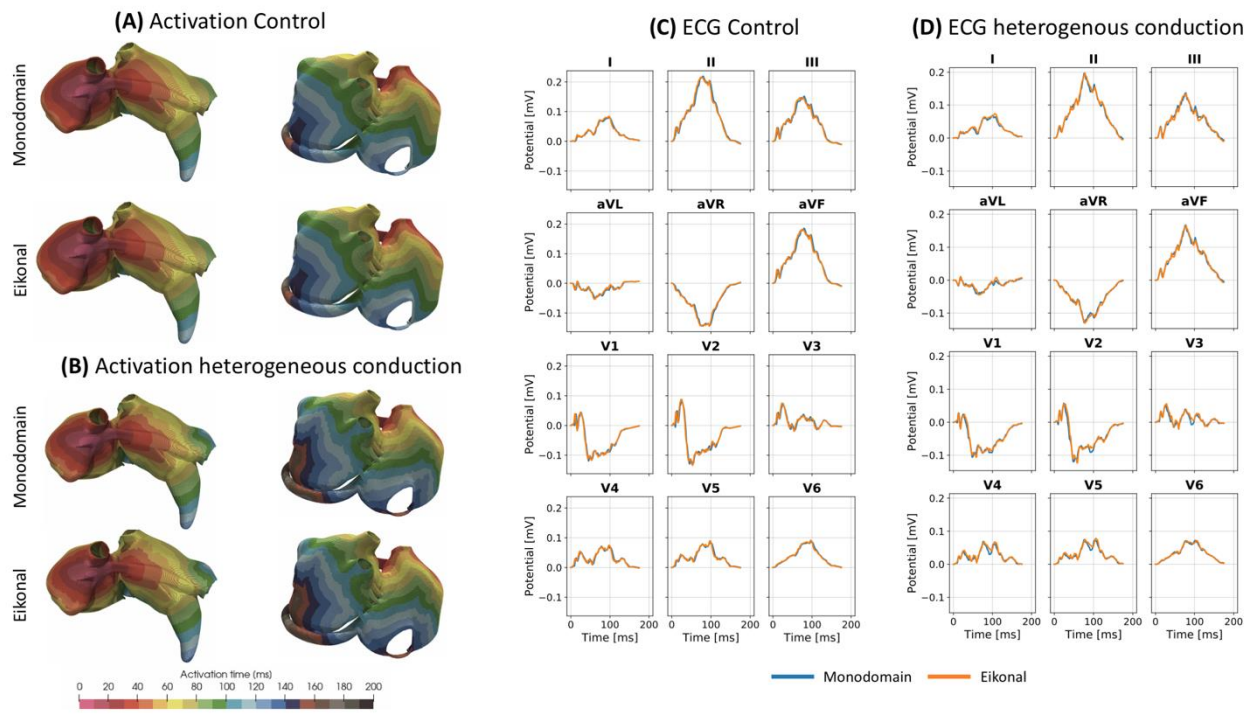


Figure 3 Comparison of the eikonal and the monodomain model, in terms of activation map (scale from 0 to 200ms) and P-wave (in mV). Activation map in control case (A) and in presence of slow conducting regions (B). P-wave in the standard 12-lead ECG in control case (C) and with slow conducting regions (D).

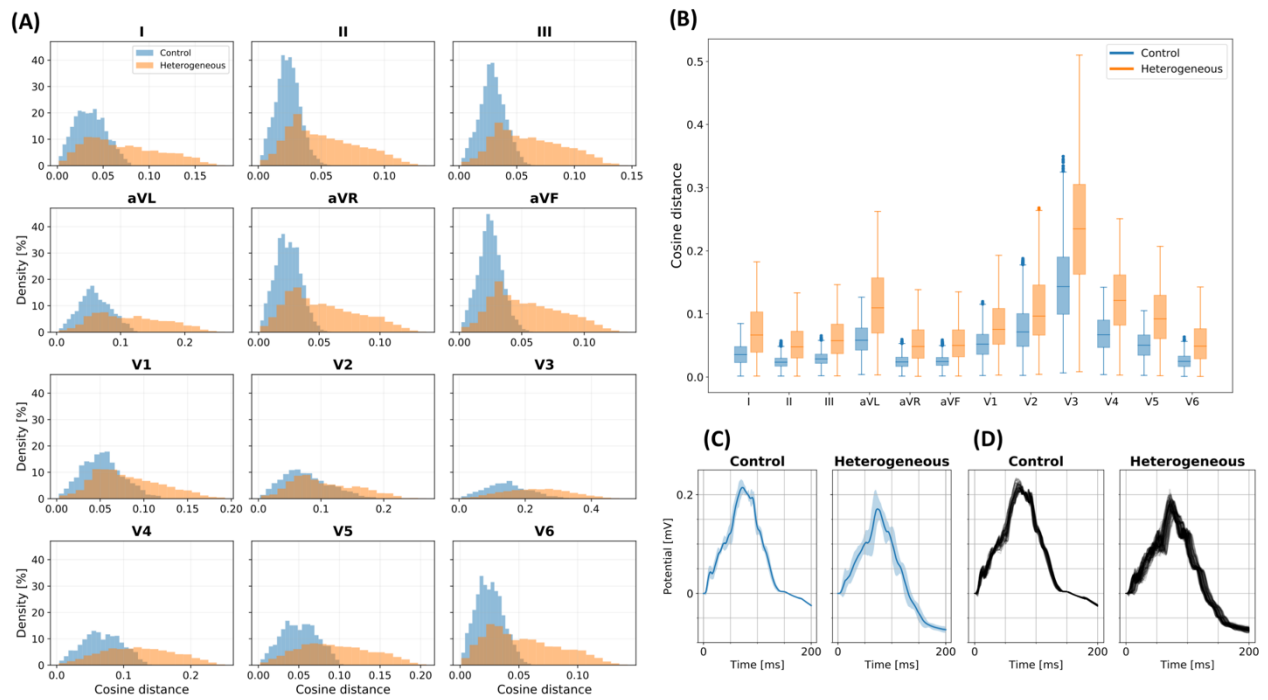


Figure 4 Comparison between P-wave beat-to-beat variability in the control case (no slow conduction regions) and in the presence of regions of heterogeneous conduction (pattern 3, 40% of slow conduction area). (A) Histogram of the entries of the cosine distance matrix in control (blue) and heterogeneous case (orange), for each ECG lead. (B) Box-plot of the cosine distance in control and heterogeneous case, for each ECG lead. (C) Lead II average P-wave with shaded ± 2 standard deviation and (D) superimposed P-waves, with EAS around SAN01 an variability of 4 mm.

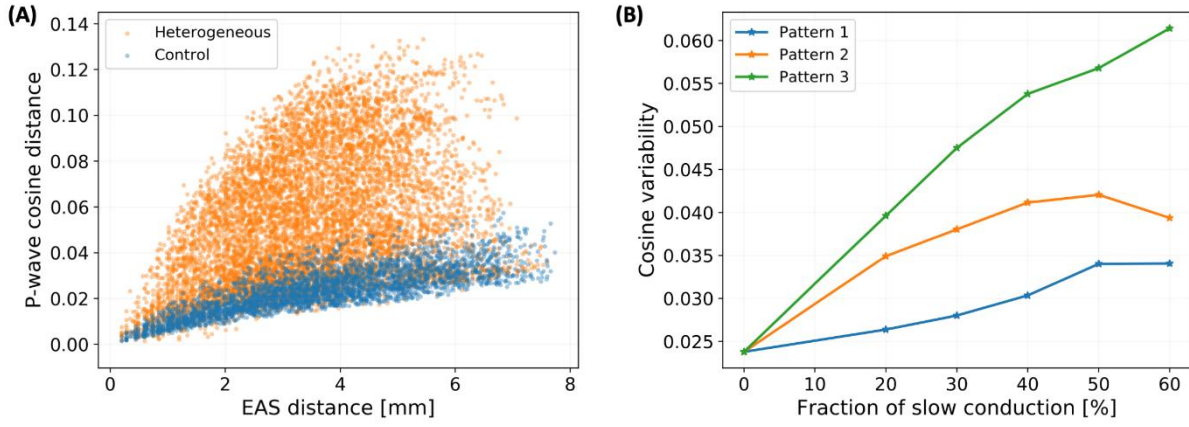


Figure 5 P-wave in lead II variability as a function of the EAS radius sampling. (A) Scatter plot between the EAS pairwise Euclidean distance, and the P-wave cosine distance, for both control and heterogeneous case. (B) P-wave variability as a function of the fraction of the slow conduction region, for 3 different patterns.



Figure 6 P-wave difference in variability between control and with heterogeneous conduction, for each lead of the 12-lead ECG and the SAN exit location. Each 12x12 grid refers to a choice of distribution (vertical) and fraction (horizontal) of the heterogeneous region. A green color box indicates that the variability in control is smaller. A red color box indicates that the variability in control is larger. The darker the color, the stronger the variability.

Table 1 Summary of the parameters for the simulations.

Parameter	Value
Surface-to-volume ratio [1/cm]	800 (1600 in slow conduction regions)
Conduction velocity scaling factor [cm/(ms mS ^{1/2})]	1.614 (reference)
Intercaval RA conductivity [mS/cm]	$\sigma_{il} = \sigma_{el} = \sigma_{it} = \sigma_{et} = 1.5$
Bachmann's bundle conductivity [mS/cm]	$\sigma_{il} = 9.0, \sigma_{el} = 9.0, \sigma_{it} = 0.9, \sigma_{el} = 3.6$
Slow conduction region conductivity [mS/cm]	$\sigma_{il} = 1.5, \sigma_{el} = 3.0, \sigma_{it} = 0.3, \sigma_{el} = 3.6$
RA and LA conductivity [mS/cm]	$\sigma_{il} = 3.0, \sigma_{el} = 3.0, \sigma_{it} = 0.9, \sigma_{el} = 3.6$
Ventricles conductivity [mS/cm]	$\sigma_{il} = 3.0, \sigma_{el} = 3.0, \sigma_{it} = 0.3, \sigma_{el} = 1.2$
Interstitial conductivity [mS/cm]	$\sigma_{el} = 2.0, \sigma_{el} = 2.0$
Lungs conductivity [mS/cm]	$\sigma_{el} = 0.5, \sigma_{el} = 0.5$
Blood conductivity [mS/cm]	$\sigma_{el} = 6.0, \sigma_{el} = 6.0$
Skeletal muscle conductivity [mS/cm]	$\sigma_{el} = 3.55, \sigma_{el} = 3.55, \sigma_{ec} = 0.44$
Atrial grid size [cm]	0.02
Torso grid size [cm]	0.1